Automated Frequency-Domain Small-Signal Stability Analysis of Electrical Energy Hubs

Francisco Javier Cifuentes Garcia, Thomas Roose, Özgür Can Sakinci, Dongyeong Lee,
Lokesh Dewangan, Eros Avdiaj and Jef Beerten
KU Leuven, Dept. Electrical Engineering (ESAT-Electa), Leuven & Etch by EnergyVille, Genk, Belgium

***Abstract*—Energy hubs will be crucial infrastructures in future power systems, enhancing renewable energy integration and flexibility. However, their stability analysis is demanding as they incorporate many converters supplied by multiple vendors, for which only black-box models are available. We address this challenge by introducing the first openly available frequency-domain stability analysis tool based on Electromagnetic Transients (EMT) software models. An efficient and reliable frequency-domain identification procedure is presented and validated, which enables the application of state-of-the-art multi-terminal stability assessment methods. The capabilities of frequency-domain methods to provide valuable stability insights are demonstrated for the novel case study of a multi-terminal hybrid energy hub, thus paving the way for their safe deployment into modern power systems.**

***Index Terms*—Energy hub, impedance-based method, AC/DC, multi-terminal, HVDC, offshore wind, MMC, nodal admittance.**

I. Introduction

Energy hubs, such as energy islands, are emerging as key components in future power systems, enabling efficient integration of renewable energy sources and flexibility [1], [2]. However, their unique electrical characteristics increase the need for detailed stability studies. For example, these hubs are expected to contain AC/DC converters from multiple vendors, raising concerns about their interoperability and contribution to system stability since their controllers are largely designed independently. Furthermore, to evaluate the dynamics of such multi-vendor systems, only black-box models are made available to protect the original equipment manufacturer's intellectual property. These models lack access to internal information, obstructing conventional small-signal stability assessment methods, e.g., state-space eigenvalue analysis.

Currently, the majority of stability studies for complex power systems are based on time-domain simulations, which imply long computational times and a considerable modelling effort without directly contributing to identifying the problem source or mitigation measures. Alternatively, frequency-domain small-signal stability analysis techniques stand out as powerful and modular alternatives for power systems with high penetration of converter-based devices, such as Offshore Wind Farms (OWF) and High-Voltage Direct Current (HVDC) transmission systems. Furthermore, they allow to perform the small-signal stability analysis of systems based on black-box models [3]. Frequency-domain methods rely on the impedance or admittance representation of power system components, which are then interconnected following Kirchhoff's circuit laws, thus forming a closed-loop feedback representation, which is used to determine system stability [4]. However, arbitrary aggregation of several individually stable components into two equivalent subsystems has proven to be inadequate as such encapsulation might result in right half-plane (RHP) poles, thereby complicating the application of the Generalised Nyquist Criterion (GNC) [5]. Therefore, interaction analysis involving HVDC converters and multi-terminal grids is not generally possible by collapsing the surrounding AC and DC subsystems. Furthermore, adequate HVDC converter representation in small-signal stability analysis requires the use of a three-port admittance matrix reflecting the converter impact on both the AC and DC-side dynamics [6]. Therefore, the commonly used multi-terminal formulation based on the nodal admittance matrix can be extended to ensure the stability of individual subsystems [7]–[10]. The authors in [10] incorporate the three-port admittance to represent two-level HVDC converters and study a hybrid AC/DC transmission system. In addition, the computation of bus and impedance participation factors (PFs) and bus observability [11] is further developed and applied to the stability analysis in the presence of power electronics in [12]–[16]. Recently, the relationship between the different impedance-based PFs and the state-space eigenvalue sensitivity is revealed in [17], [18].

Nevertheless, the stability of hybrid AC/DC multi-terminal grids has not yet been studied by means of the nodal admittance matrix method and representing the HVDC converters via their three-port admittance. Moreover, most studies adopt the simplified two-level converter topology to represent HVDC converters, whilst the Modular Multilevel Converter (MMC) is currently the industry standard for HVDC projects. Additionally, at present, no open-source tools are available to perform the aforesaid state-of-the-art stability analysis.

This paper addresses these research gaps in the stability studies of AC/DC power systems by enabling a modular frequency-domain stability assessment procedure. The procedure starts by characterising the frequency-domain admittance of any subsystem defined at target nodes, including black-box components, and then integrating them into a state-of-the-art multi-terminal formulation, which reveals critical information, such as the frequency of interactions and participating buses. The method's effectiveness is demonstrated for the first time on an electrical

Corresponding author: franciscojavier.cifuentesgarcia@kuleuven.be

979-8-3503-9042-1/24$31.00 ©2024 IEEE

energy hub, including a multi-terminal MMC-based HVDC network with both AC and DC interconnections in parallel. We provide the first openly available tool[1] fully automating the complete small-signal stability analysis for models developed in the commercial Electromagnetic Transient (EMT) software PSCAD, and thus enabling a detailed study of hybrid AC/DC systems. Our results thoroughly validate the implemented system identification and stability assessment methods, as well as demonstrate the interaction identification and mitigation capabilities in a novel energy hub case study.

The rest of the paper is organised as follows. Section II revisits the stability analysis methodology for AC/DC systems. Next, Section III introduces the frequency-domain identification method based on EMT models, which is validated via analytical models. Subsequently, Section IV presents the stability analysis of a representative electrical energy hub. Lastly, the main contributions are summarized in Section V.

II. Methodology for the small-signal stability assessment of hybrid AC/DC systems

The classical impedance-based stability analysis relies on the partition of the system at a single terminal into a source and load subsystem, represented by their small-signal impedance matrices $\boldsymbol{Z}_s(s)$ and $\boldsymbol{Z}_l(s)$ respectively, where $s = j\omega$ is the Laplace complex frequency [19]. The connection of these two subsystems can be formulated as a closed-loop feedback system with loop gain matrix $\boldsymbol{L}(s) = \boldsymbol{Z}_s(s)\boldsymbol{Z}_l^{-1}(s)$, whose stability can be assessed based on the GNC by checking whether the (-1, 0j) point in the Nyquist plot of $\boldsymbol{L}(s)$ is encircled (unstable) or not (stable) [3]–[5]. However, this approach may lead to an incorrect stability assessment if multiple devices are aggregated within each subsystem, e.g. electrical energy hubs. The reason is that the impedance-based method assumes that the two subsystems are individually stable, but aggregating multiple converters and other components in the subsystems might lead to an unstable representation due to adverse interactions or to RHP zeros in $\boldsymbol{Z}_l(s)$ [5], [20]. Hence, an analytical system representation is required to know the number of RHP poles of $\boldsymbol{L}(s)$ for an accurate stability assessment based on the GNC, thus preventing the use of black-box models. To overcome that limitation, alternative methods have been proposed recently based on splitting the system at multiple locations to ensure no RHP poles in the loop gain matrix [5], [9], [10], [16], thereby allowing a precise stability assessment of systems incorporating black-box models. The following subsections revisit the formulation and characteristics of said state-of-the-art method.

A. Stability analysis by split in node and edge subsystems

To avoid RHP poles in the loop gain matrix, a node and edge subsystem are defined at multiple splitting terminals. This approach is depicted in Fig. 1 for a hybrid AC/DC power system, where AC and DC networks are interconnected through multiple HVDC converters. The node subsystem (gray area) contains the converters, sources and loads, connected at the splitting nodes. These nodes are interconnected through the DC and AC networks, which are included in the edge subsystem (white area). As the elements in the node subsystem are standalone stable, this system partition ensures no RHP poles in their corresponding admittance form. Simultaneously, the edge subsystem representation does not present RHP poles or zeros as it only includes passive components [5], [9], [10]. Subsequently, the small-signal stability of the whole system can be assessed by applying the GNC based on the closed-loop formed by the node and edge subsystems.

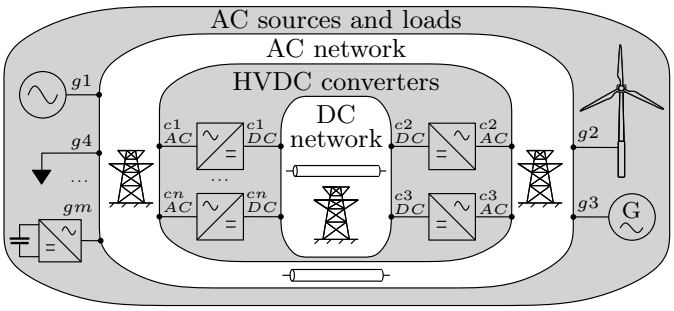

Fig. 1. General representation of AC/DC power systems. Definition of node (converters, sources and loads) and edge (DC and AC network) subsystems, in grey and white, respectively.

The edge subsystem is represented by the edge admittance matrix $\boldsymbol{Y}_{edge}(s)$, giving the relation between the node currents and voltages, i.e $\Delta\boldsymbol{I}(s)$ and $\Delta\boldsymbol{V}(s)$ respectively,

$$\Delta\boldsymbol{I}(s) = \boldsymbol{Y}_{edge}(s)\Delta\boldsymbol{V}(s). \tag{1}$$

Vectors and matrices are noted in bold and Δ indicates small-signal perturbations of the variables. All variables are expressed in the frequency domain unless explicit time-dependency is indicated, and thus the Laplace variable might be omitted for compactness. The voltages and currents at the terminals of the n HVDC converters and m sources/loads, distinguished by the subscript c and g, respectively, are

$$\Delta\boldsymbol{V} = [\Delta\boldsymbol{v}_{c1}^T \cdots \Delta\boldsymbol{v}_{cn}^T \;\; \Delta\boldsymbol{v}_{g1}^T \cdots \Delta\boldsymbol{v}_{gm}^T]^T \tag{2a}$$

$$\Delta\boldsymbol{I} = [\underbrace{\Delta\boldsymbol{i}_{c1}^T \cdots \Delta\boldsymbol{i}_{cn}^T}_{\text{HVDC converters}} \;\; \underbrace{\Delta\boldsymbol{i}_{g1}^T \cdots \Delta\boldsymbol{i}_{gm}^T}_{\text{Sources and loads}}]^T \tag{2b}$$

where the superscript T denotes non-conjugate transposition. Each vector, $\boldsymbol{i}_{gi}, \boldsymbol{v}_{gi}$, $i \in \{1, m\}$, of size 2×1 represents positive-negative sequence or *dq*-frame quantities. In addition, HVDC converters vectors of size 3×1 also include the corresponding DC-side quantities. Moreover, the converters, sources, and loads are modelled by their Norton equivalent,

$$\Delta\boldsymbol{I} = \Delta\boldsymbol{I}_N - \boldsymbol{Y}_{node}\Delta\boldsymbol{V}, \tag{3}$$

where $\boldsymbol{I}_N$ represents current disturbances at the nodes,

$$\Delta\boldsymbol{I}_N = \left[\Delta\boldsymbol{i}_{N,c1}^T \cdots \Delta\boldsymbol{i}_{N,cn}^T \quad \Delta\boldsymbol{i}_{N,g1}^T \cdots \Delta\boldsymbol{i}_{N,gm}^T\right]^T. \tag{4}$$

The node admittance matrix $\boldsymbol{Y}_{node}$ is a block diagonal matrix in which the elements are defined by the individual converters, sources, and loads small-signal admittance matrices,

$$\boldsymbol{Y}_{node} = \text{blkdiag}[\underbrace{\boldsymbol{Y}_{c1} \cdots \boldsymbol{Y}_{cn}}_{\text{HVDC converters}} \;\; \underbrace{\boldsymbol{Y}_{g1} \cdots \boldsymbol{Y}_{gm}}_{\text{Sources and loads}}] \tag{5}$$

[1]The tool is freely available in https://www.esat.kuleuven.be/electa/ztool

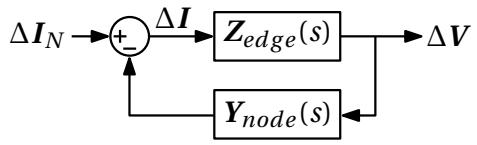

Fig. 2. Feedback formed by the node and edge subsystems.

Combining (1) and (3) gives the multiple-input multiple-output (MIMO) closed-loop representation shown in Fig. 2,

$$\Delta \boldsymbol{V} = \left(\boldsymbol{I} + \boldsymbol{Z}_{edge}\boldsymbol{Y}_{node}\right)^{-1} \boldsymbol{Z}_{edge}\Delta \boldsymbol{I}_N, \tag{6}$$

where $\boldsymbol{Z}_{edge}$ is the inverse of $\boldsymbol{Y}_{edge}$. The loop gain matrix of the closed-loop system is then defined as

$$\boldsymbol{L}(s) = \boldsymbol{Z}_{edge}(s)\boldsymbol{Y}_{node}(s). \tag{7}$$

Then, the small-signal stability can be assessed based on the Generalized Nyquist Criterion (GNC) by evaluating the Nyquist plot of $\boldsymbol{L}(s)$. The GNC, rooted in the argument principle, states that a system is stable if and only if the eigenloci of $\boldsymbol{L}(s)$, taken together, encircle the (-1, 0j) point P times counterclockwise in the Nyquist plot, assuming that there are no hidden unstable modes and with P the number of RHP poles of $\boldsymbol{L}(s)$ counting multiplicities [21]. The eigenloci are the eigenvalues of the loop gain matrix evaluated over the entire frequency range, i.e. $\lambda_i(\boldsymbol{L}(j\omega))$. Considering the system split previously described, the edge subsystem $\boldsymbol{Z}_{edge}(s)$ only consists of passive network elements which are stable, e.g. transmission lines. Furthermore, the block-diagonal elements of $\boldsymbol{Y}_{node}(s)$ contain no RHP poles as the converters, generators and loads are individually stable. Hence, $\boldsymbol{L}(s)$ has no RHP poles, i.e. $P = 0$. Therefore, the whole system is stable according to the GNC if no eigenloci encircle the (-1, 0j) point, which enables the use of black-box models as the eigenloci can be plotted based on the frequency response data of $\boldsymbol{L}(s)$.

B. System oscillation modes and participation factor analysis

Equivalent to the eigenvalue analysis in the state-space framework, it is possible to determine the oscillation modes from the frequency-domain MIMO closed-loop description. These modes provide insights into the oscillatory behaviour of the node voltages and causes of system interactions. The oscillation identification is based on the closed-loop bus impedance matrix, $\boldsymbol{Z}_{bus}^{cl}$, which is the inverse of the conventional nodal admittance matrix, $\boldsymbol{Y}_{bus}^{cl}$, and relates small-signal current disturbances at the nodes and resulting node voltage variations. This matrix is calculated by rewriting (6) as (8),

$$\Delta \boldsymbol{V} = \left(\boldsymbol{Y}_{edge} + \boldsymbol{Y}_{node}\right)^{-1} \Delta \boldsymbol{I}_N = \boldsymbol{Z}_{bus}^{cl}\Delta \boldsymbol{I}_N. \tag{8}$$

The system oscillation modes are then determined by applying the eigenvalue decomposition (EVD) of $\boldsymbol{Z}_{bus}^{cl}(s)$ at every frequency of interest $s = j\omega$ [11]. Note that, contrary to the state-space eigenvalue analysis, the EVD of $\boldsymbol{Z}_{bus}^{cl}(j\omega)$ is now evaluated in the frequency domain and calculated at a particular frequency within a range of interest,

$$\boldsymbol{Z}_{bus}^{cl}(j\omega) = \boldsymbol{\Phi}(j\omega)\boldsymbol{\Lambda}(j\omega)\boldsymbol{\Psi}(j\omega), \tag{9}$$

where $\boldsymbol{\Lambda}(j\omega)$ is the diagonal eigenvalue matrix and $\boldsymbol{\Phi}(j\omega)$ and $\boldsymbol{\Psi}(j\omega)$ the right and left eigenvector matrices respectively. The main oscillation modes are then identified based on the peak absolute values of the eigenvalues $|\lambda_i(j\omega)|$ [11]. To gain additional insights in the cause of adverse interactions, the observability, controllability, and participation factors (PFs) can be calculated for a particular oscillation mode [13], [22]. The participation factor $P_{ki}(j\omega_m)$ indicates the contribution of terminal k to the oscillation mode i with frequency ω_m, and can be calculated as (10). Contrary to the state-space framework, the contribution of particular control loops or components to the oscillation modes cannot be easily determined via these PFs since additional calculations are needed [18]. Nevertheless, only frequency response data is needed to determine these PFs and thus they can identify possible instability causes while being compatible with black-box models.

$$P_{ki}(j\omega_m) = \frac{|\phi_{ki}(j\omega_m)\psi_{ik}(j\omega_m)|}{\sum_{k=1}^{N}|\phi_{ki}(j\omega_m)\psi_{ik}(j\omega_m)|} \tag{10}$$

III. Frequency domain admittance identification

This section presents a general approach for frequency-domain characterization of AC/DC systems suited for the direct application of the small-signal stability assessment described in previous Section II. Firstly, Section III-A revisits the generalities of the scanning procedure. Secondly, Section III-B clarifies the adopted method to efficiently construct the node admittance matrix $\boldsymbol{Y}_{node}(s)$ containing sources, loads and converters. Next, Section III-C introduces the proposed approach to compute the edge impedance matrix $\boldsymbol{Z}_{edge}(s)$ of the meshed AC/DC networks interconnecting sources, loads and converters. Lastly, Section III-D presents the validation of the scan procedure for a selected number of relevant components.

A. Generalities of the identification procedure

The stability analysis described in Section II relies on the admittance of the subsystems under study as seen from each bus. In other words, the subsystems need to be decoupled at their terminals without altering their operating point. Contrary to shunt current injections or series voltage perturbation [23], we achieve the decoupling by connecting controlled shunt voltage sources. The voltage sources need to be ideal, i.e. they present zero impedance, and controlled to reproduce the steady-state fundamental frequency voltage waveform at the terminal. Therefore, the operating point of each subsystem is unaltered, which is of importance for non-linear devices whose characteristics change with the operating point, e.g. HVDC converters. After the decoupling, a snapshot can be taken to resume subsequent simulations, avoiding the initialisation transient. Next, the system needs to be excited so as to characterize its small-signal dynamics. There are many approaches for perturbation-based impedance identification differing in the frame and type of perturbation and measurement for which a thorough review can be found in [24]. In this paper, the single-frequency perturbation in the *dq*-frame is adopted because of its simplicity in simulation environments, minimization of inaccurate results related to frequency coupling with respect to multi-frequency methods and ease of integration into the stability analysis framework. At every frequency, the admittance matrix computation is based on solving a linear system

of equations considering that in an M-dimensional space, a linearly independent set can have at most M vectors. In particular, $M = 2$ for AC sources/loads in the *d,q* frame, whereas $M = 3$ in the *dc,d,q* frame for HVDC converters. To ensure linearly independent perturbations at AC buses, the *d*-axis voltage is aligned with phase *a*, and only *d*-axis or *q*-axis voltage perturbations are applied separately. Therefore, every subsystem is excited at every frequency with as many linearly independent perturbations as the degrees of freedom of its small-signal representation. The simulations are run in parallel using multiple cores to reduce the computation time. Once the subsystems reach sinusoidal steady state, the single-sided FFT is applied to the small-signal currents and voltages and the response at the target frequency is retrieved to compute the corresponding admittance matrix. This is illustrated in Fig. 3 with the *d*-axis voltage of a MMC station, where the perturbation at 200 Hz results in one of the three independent perturbation sets and associated currents.

B. Node admittance matrix identification

The node admittance is built by identifying each block diagonal matrix, corresponding to HVDC converters or sources/loads. The sources/loads are interfaced to the system at a single AC three-phase connection point. This allows to perturb each bus independently and in parallel at a given frequency. Therefore, all sources/loads can be identified simultaneously, which considerably improves the simulation time. The *dq*-frame admittance of each source/load is given by (11),

$$\boldsymbol{Y}_{d,q}(s) = \begin{bmatrix} \Delta i_1^d(s) & \Delta i_2^d(s) \\ \Delta i_1^q(s) & \Delta i_2^q(s) \end{bmatrix} \begin{bmatrix} \Delta v_1^d(s) & \Delta v_2^d(s) \\ \Delta v_1^q(s) & \Delta v_2^q(s) \end{bmatrix}^{-1}, \quad (11)$$

where the subscript 1 and 2 refer to the values of each linearly independent set of perturbations, e.g. the perturbation $\Delta v_1^d \neq 0$ and $\Delta v_1^q = 0$ result in the currents Δi_1^d and Δi_1^q. HVDC converters are also interfaced at their DC-side so three linearly independent voltage perturbations are applied, two at the AC-side as previously described for sources/loads and an additional one at the DC-side, while all currents are recorded. Consequently, the 3×3 HVDC converter admittance is computed by (12), where the subscripts refer to each linearly independent set of perturbations, which are practically implemented as separated *d*, *q* and *dc* voltage perturbations.

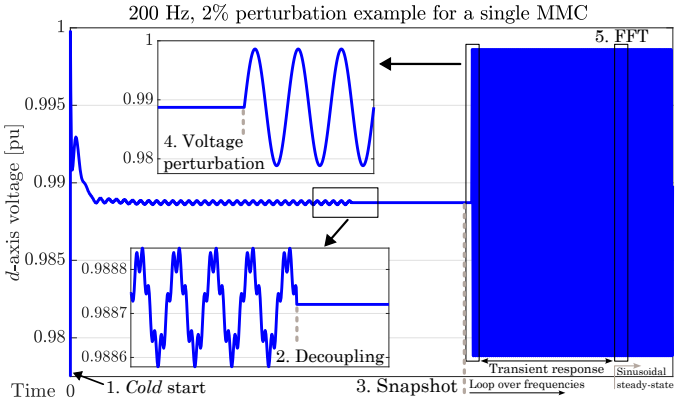

Fig. 3. Illustration of a single-frequency voltage perturbation.

$$\boldsymbol{Y}_{dc,d,q} = \begin{bmatrix} \Delta i_1^{dc} & \Delta i_2^{dc} & \Delta i_3^{dc} \\ \Delta i_1^d & \Delta i_2^d & \Delta i_3^d \\ \Delta i_1^q & \Delta i_2^q & \Delta i_3^q \end{bmatrix} \begin{bmatrix} \Delta v_1^{dc} & \Delta v_2^{dc} & \Delta v_3^{dc} \\ \Delta v_1^d & \Delta v_2^d & \Delta v_3^d \\ \Delta v_1^q & \Delta v_2^q & \Delta v_3^q \end{bmatrix}^{-1} \quad (12)$$

Note that the adopted scan procedure returns each admittance matrix, $\boldsymbol{Y}_{d,q}(s)$ and $\boldsymbol{Y}_{dc,d,q}(s)$, in their own local reference frame. Therefore, in order to build the node admittance matrix as in (5), each matrix is rotated to a common (global) reference frame based on the steady-state voltage angle at each bus. For a *dq*-frame with *q*-axis lagging the rotation in (13) is used for HVDC converters, where the rotation angle, $\delta_i = \theta_i - \theta_{ref}$, is the difference between the angle of each bus, θ_i, and that of the reference bus, θ_{ref} [5]. The reference angle, θ_{ref}, can be arbitrarily set to that of one bus of each AC area, e.g. the steady-state power flow reference bus. The rotation matrix for AC sources and loads is obtained by removing the first column and row from $\boldsymbol{R}_i$ in (13).

$$\boldsymbol{R}_i = \begin{bmatrix} 1 & 0 & 0 \\ 0 & \cos\delta_i & -\sin\delta_i \\ 0 & \sin\delta_i & \cos\delta_i \end{bmatrix}, \quad \boldsymbol{Y}_{ci} = \boldsymbol{R}_i^{-1}\boldsymbol{Y}_i\boldsymbol{R}_i. \quad (13)$$

C. Edge admittance identification of AC and DC networks

The computation of the edge admittance matrix at each angular frequency differs from that of the node admittance in the required number of independent perturbations since it interconnects multiple buses. For an arbitrary DC network with N target buses, the edge admittance matrix is of size $N \times N$. Therefore, N linearly independent perturbation sets are needed at each frequency, noted by the subscript $1, ..., N$. A sinusoidal perturbation can be applied at each target bus while the others remain unaltered to obtain N-linearly independent sets. After reaching sinusoidal steady state, the FFT is applied to retrieve the target frequency response from the small-signal currents and voltages at every node, noted by the superscript $I, ..., N$. Lastly, the admittance is computed at each frequency by (14).

$$\boldsymbol{Y}_{edge} = \begin{bmatrix} \Delta i_1^I & \dots & \Delta i_N^I \\ \vdots & \ddots & \vdots \\ \Delta i_1^N & \dots & \Delta i_N^N \end{bmatrix} \begin{bmatrix} \Delta v_1^I & \dots & \Delta v_N^I \\ \vdots & \ddots & \vdots \\ \Delta v_1^N & \dots & \Delta v_N^N \end{bmatrix}^{-1} \quad (14)$$

The system topology information is needed to select the involved perturbations, to record the target currents and voltages and to reduce the number of perturbation sets for decoupled AC/DC networks, e.g. different synchronous areas. The extension of (14) for AC networks simply follows by doubling the dimensionality because the dynamics of balanced three-phase systems are fully captured in the *dq*-frame. The reference frame rotation can be omitted for the interconnecting AC networks as they are typically *dq*-symmetric [5]. Under this assumption, the number of perturbations to identify the $\boldsymbol{Y}_{edge}$ of an M-terminal meshed AC network halves from $2M$ to M. In addition, if $\boldsymbol{Y}_{edge}$ is solely made of passive components, then it is operating point independent, which allows to identify $\boldsymbol{Y}_{edge}$ once for each topology. Implementing previous considerations significantly reduces the $\boldsymbol{Y}_{edge}$ computation time.

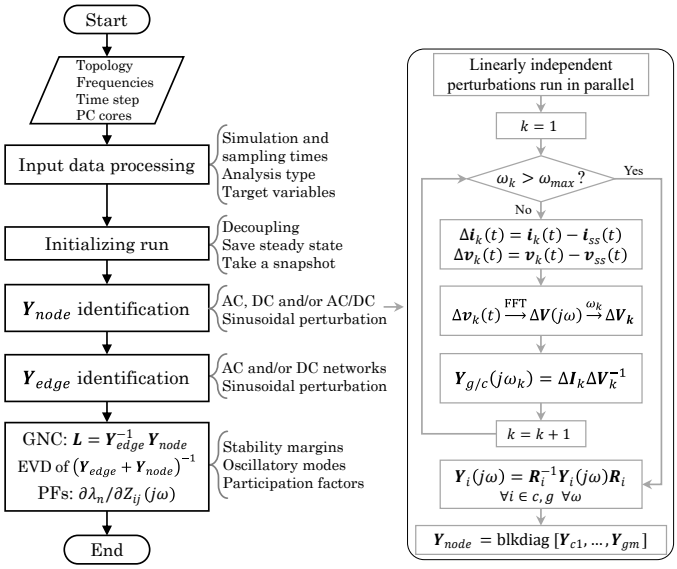

Fig. 4. Procedure summary and Y_{node} identification detail.

D. Admittance identification validation

The presented procedure is validated in Fig. 5 by comparing the analytical admittances (lines) with respect to the scans of the corresponding non-linear models in PSCAD (black dots). Fig. 5a and Fig. 5b show the admittance of a thermal power plant and an aggregated OWF with frequency and voltage support, respectively. Fig. 5c presents the admittance of the 3-terminal DC network in Fig. 6 given by its analytical wide-band model (lines) and by the EMT scan (dots). Lastly, the DC-side admittance of a grid-following MMC-based HVDC station is shown in Fig. 5d under four typical control modes: constant power (red), constant DC voltage (green), voltage-power droop with (cyan) and without (magenta) total energy control. The cable data and MMC modelling details and electrical parameters can be found in [25]. All admittances identified using the described EMT-based scan built into the tool[1] show an excellent match with the analytical models.

IV. Energy Hub Multi-Terminal Stability Analysis

The complete methodology based on EMT models outlined in Fig. 4 is demonstrated for the energy hub in Fig. 6 by validating the frequency-domain analysis with time-domain simulations. The system includes both AC and DC interconnections in parallel, an OWF and a three-terminal MMC-based HVDC grid interconnecting two AC grids. Firstly, the system is split at every bus resulting in the node and edge subsystems highlighted in Fig. 6 in grey and white, respectively. The node matrix contains the rightmost AC subsystem at bus $g1$, the OWF at bus $g2$, the AC equivalent subsystem at bus $g3$, and the three MMCs connected at buses $c1$, $c2$, and $c3$, respectively. The edge matrix contains the AC and DC networks interconnecting aforesaid nodes, i.e. overhead lines, cables, and shunt compensation. For simplicity, the two AC Thévenin equivalents and both Q-compensations are the same. Next, the frequency-domain edge and node matrices are identified from the EMT models as explained in Section III. Then, the GNC is applied to the loop-gain matrix to assess the stability

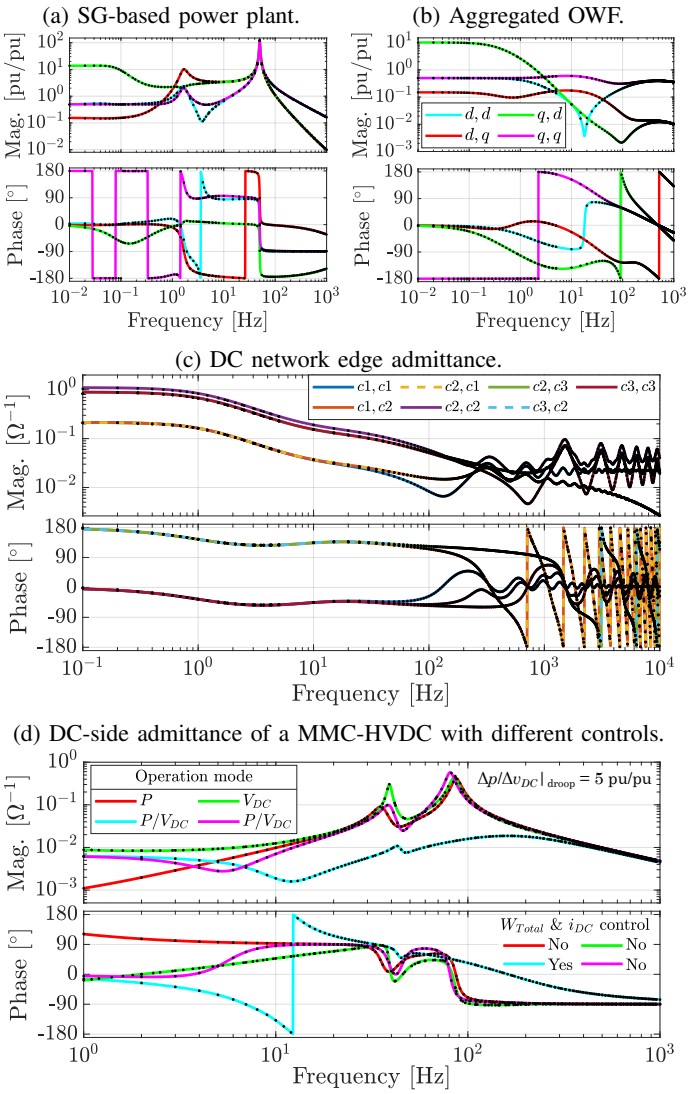

Fig. 5. Analytical admittances (lines) and EMT scan (dots).

as shown in Fig. 7a. The result indicates an unstable system as the critical point is encircled. The oscillation identification based on the EVD of the closed-loop impedance is presented in Fig. 8a, which indicates a dominant mode around 63 Hz. The PF of AC-bus $c2$ in this mode is 0.37, which is one of the highest. Likewise, the DC node $c2$ has the highest PF out of the three DC nodes. Modifying the power control settings of the

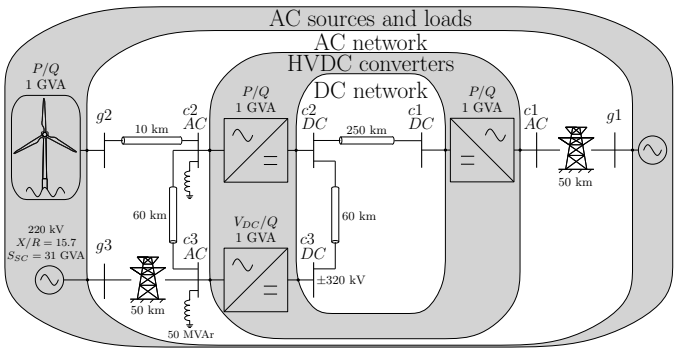

Fig. 6. Energy hub under study: node and edge subsystems.

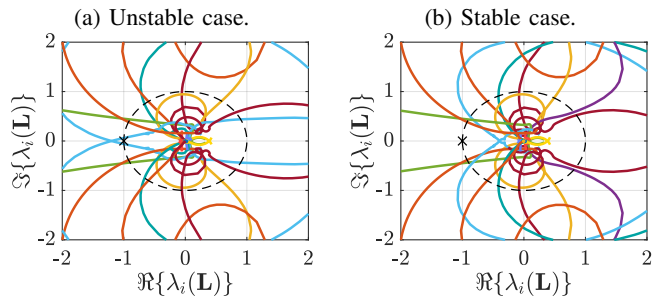

Fig. 7. Stability assessment via Generalized Nyquist Criterion.

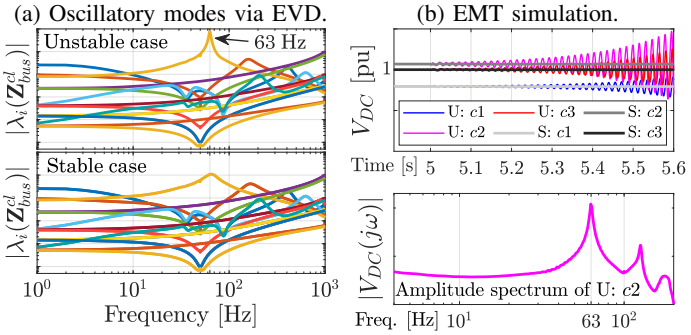

Fig. 8. Oscillation mode identification and EMT validation.

MMC at $c2$ solves the instability as verified by the eigenloci in Fig. 7b. To validate previous analysis, the DC voltages at $c1$, $c2$ and $c3$ are shown in Fig. 8b when a small load is connected at bus $c3$ after 5 s. This triggers the predicted 63 Hz oscillatory instability in the first case, as seen by the voltages labeled with U in Fig. 8b for which $c2$ has the expected largest amplitude, while the system is stable in the second case, noted by S.

V. Conclusion

Studying system stability in the presence of new and complex multi-vendor components entails additional challenges due to the nature of black-box models. Therefore, we introduce a modular frequency-domain stability assessment procedure fully automated in an open tool[1] for models in the EMT software PSCAD. The tool, validated with respect to analytical models, characterizes any subsystem in the frequency domain, including black-box components, and integrates them into a state-of-the-art MIMO formulation. Its capabilities to reveal oscillation frequencies and assess system stability are demonstrated on an electrical energy hub. This is the first openly accessible frequency-domain stability tool offering a complete automated analysis for multi-terminal AC/DC systems.

Acknowledgment

This work has received support from the Belgian Energy Transition Fund, FOD Economy, project DIRECTIONS, and project *Innovative solutions for underground high-voltage lines and grids*, funded by the Flemish Government.

References

[1] Elia, "Elia presents its plans for an energy island: the princess elisabeth island," Oct 2022, Available online.
[2] Energinet, "Offshore energy hubs - high level system description and requirements," Feb 2023, Available online.
[3] M. Amin and M. Molinas, "Small-signal stability assessment of power electronics based power systems: A discussion of impedance- and eigenvalue-based methods," *IEEE Trans. Ind. Appl.*, vol. 53, no. 5, pp. 5014–5030, Sep. 2017.
[4] M. Cheah-Mane, A. Egea-Alvarez, E. Prieto-Araujo, H. Mehrjerdi, O. Gomis-Bellmunt, and L. Xu, "Modeling and analysis approaches for small-signal stability assessment of power-electronic-dominated systems," *WIREs Energy and Environment*, vol. 12, no. 1, p. e453, 2023.
[5] C. Zhang, M. Molinas, A. Rygg, and X. Cai, "Impedance-based analysis of interconnected power electronics systems: Impedance network modeling and comparative studies of stability criteria," *IEEE J. Emerg. Sel. Top. Power Electron.*, vol. 8, no. 3, pp. 2520–2533, Sep. 2020.
[6] S. Shah and L. Parsa, "Impedance modeling of three-phase voltage source converters in dq, sequence, and phasor domains," *IEEE Transactions on Energy Conversion*, vol. 32, no. 3, pp. 1139–1150, 2017.
[7] E. Ebrahimzadeh, F. Blaabjerg, X. Wang, and C. L. Bak, "Harmonic stability and resonance analysis in large pmsg-based wind power plants," *IEEE Transactions on Sustainable Energy*, vol. 9, no. 1, pp. 12–23, 2018.
[8] H. Liu, X. Xie, and W. Liu, "An oscillatory stability criterion based on the unified *dq* -frame impedance network model for power systems with high-penetration renewables," *IEEE Trans. Power Syst.*, vol. 33, 2018.
[9] Y. Li, Z. Shuai, X. Liu, Y. Chen, Z. Li, Y. Hong, and Z. J. Shen, "Stability analysis and location optimization method for multiconverter power systems based on nodal admittance matrix," *IEEE J. Emerg. Sel. Top. Power Electron.*, vol. 9, no. 1, pp. 529–538, 2021.
[10] J. Pedra, L. Sainz, and L. Monjo, "Three-port small signal admittance-based model of VSCs for studies of multi-terminal HVDC hybrid AC/DC transmission grids," *IEEE Trans. Power Syst.*, vol. 36, no. 1, pp. 732–743, Jan. 2021.
[11] W. Xu, Z. Huang, Y. Cui, and H. Wang, "Harmonic resonance mode analysis," *IEEE Trans. Power Del.*, vol. 20, no. 2, Apr. 2005.
[12] Y. Zhu, Y. Gu, Y. Li, and T. C. Green, "Participation analysis in impedance models: The grey-box approach for power system stability," *IEEE Trans. Power Syst.*, vol. 37, no. 1, pp. 343–353, 2022.
[13] Y. Liao, X. Wang, and X. Wang, "Frequency-domain participation analysis for electronic power systems," *IEEE Transactions on Power Electronics*, vol. 37, no. 3, pp. 2531–2537, 2022.
[14] Y. Zhang, D. Duckwitz, N. Wiese, and M. Braun, "Extended nodal admittance matrix based stability analysis of hvdc connected ac grids," *IEEE Access*, 2022.
[15] L. Orellana, L. Sainz, E. Prieto-Araujo, M. Cheah-Mané, H. Mehrjerdi, and O. Gomis-Bellmunt, "Study of black-box models and participation factors for the positive-mode damping stability criterion," *International Journal of Electrical Power & Energy Systems*, vol. 148, 2023.
[16] Y. Liao, H. Wu, X. Wang, M. Ndreko, R. Dimitrovski, and W. Winter, "Stability and sensitivity analysis of multi-vendor, multi-terminal hvdc systems," *IEEE Open J. Power Electron.*, vol. 4, pp. 52–66, 2023.
[17] Y. Zhu, Y. Gu, Y. Li, and T. C. Green, "Impedance-based root-cause analysis: Comparative study of impedance models and calculation of eigenvalue sensitivity," *IEEE Trans. Power Syst.*, vol. 38, no. 2, 2023.
[18] C. Zhang, H. Zong, X. Cai, and M. Molinas, "On the relation of nodal admittance- and loop gain-model based frequency-domain modal methods for converters-dominated systems," *IEEE Trans. Power Syst.*, vol. 38, no. 2, pp. 1779–1782, 2023.
[19] R. Middlebrook, "Input filter considerations in design and application of switching regulators," in *Proc. IEEE IAS Annual Meeting*, Chicago, USA, Oct. 1976, pp. 366–382.
[20] T. Roose, A. Lekić, M. M. Alam, and J. Beerten, "Stability analysis of high-frequency interactions between a converter and HVDC grid resonances," *IEEE Trans. Power Deliv.*, vol. 36, no. 6, Dec. 2021.
[21] J. Maciejowski, *Multivariable feedback design*. Addison-Wesley, 1989.
[22] E. Ebrahimzadeh, F. Blaabjerg, X. Wang, and C. L. Bak, "Bus participation factor analysis for harmonic instability in power electronics based power systems," *IEEE Trans. Power Electron.*, vol. 33, no. 12, pp. 10 341–10 351, Dec. 2018.
[23] D. Yang, X. Wang, M. Ndreco, W. Winter, R. Juhlin, and A. Krontiris, "Automation of Impedance Measurement for Harmonic Stability Assessment of MMC-HVDC Systems," 2019, 18th Wind Integration Workshop.
[24] J. Pedra, L. Sainz, and L. Monjo, "Review and Improvements to the Measurements of the VSC Impedance Transfer Matrix," *IEEE Trans. Power Del.*, vol. 39, no. 2, pp. 1283–1298, 2024.
[25] Özgür Can Sakinci, A. Lekić, and J. Beerten, "Generalized impedance-based AC/DC power system modeling for harmonic stability analysis," *Int. J. Elec. Power (IJEPES)*, vol. 143, p. 108456, 2022.